Calibrating Electro-Optic Sampling Systems*

Dylan F. Williams, Paul D. Hale, Tracy S. Clement, and Juanita M. Morgan

National Institute of Standards and Technology, 325 Broadway, Boulder, CO 80305

***Abstract*- We apply frequency-domain impedance mismatch corrections to a temporal electro-optic sampling system and use it to characterize the magnitude and phase response of a photoreceiver that is physically far removed from the point where the voltage waveforms are measured. We identify and evaluate additional sources of measurement uncertainty.**

I. Introduction

In this paper we present unique frequency-domain impedance mismatch corrections and error estimates for temporal electro-optic sampling systems. The mismatch corrections, which we presented in [1], allow us to determine Thévenin and Norton equivalent circuits for electrical sources, as well as the voltage they would deliver to an ideal 50 Ω load. We apply the system to characterizing a photoreceiver.

Figure 1 shows a schematic diagram of our electro-optic sampling system, which is similar to those described in [2]. The laser produces a train of roughly 100 fs long pulses in an open collimated beam. We split the laser output into two beams: an "excitation" beam, and a "sampling" beam. We use the excitation beam to excite the photoreceiver that we wish to characterize. The photoreciever has an optical input and a coaxial electrical output. It consists of a short length of optical input fiber, a photodiode, biasing circuit, and electrical matching network.

When illuminated by the optical excitation beam, the photoreceiver creates a series of electrical impulses at its coaxial output. The pulses in the optical excitation beam are so short, compared to the response time of the photoreceiver, that the electrical signals generated by the photoreceiver are nearly equal to the receiver's electrical impulse response that we would like to measure.

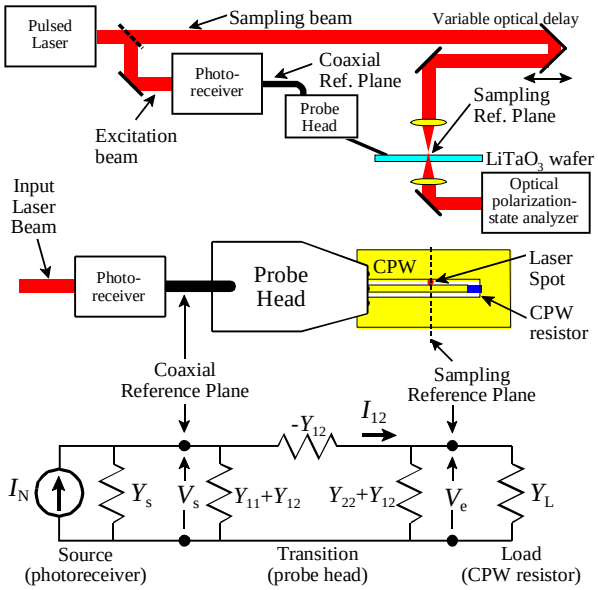

Fig. 1. A schematic diagram of our electro-optic sampling system (top), a top-view schematic (center), and an electrical equivalent circuit (bottom).

The electrical impulses generated by the photoreceiver propagate through the probe head and down to a coplanar waveguide (CPW) fabricated on an electro-optic y-cut $LiTaO_3$ wafer 0.5 mm thick. The direction of propagation in the CPW is parallel to the x-axis of the $LiTaO_3$ wafer. The probe head, CPW, and CPW termination in the electro-optic sampling system distort the electrical impulses emanating from the photoreceiver.

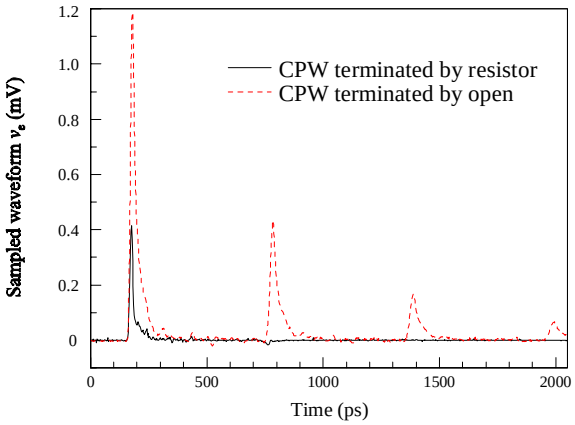

Fig. 2. Two waveforms measured by our electro-optic sampling system. Except for the two CPW terminations, all of the conditions in the experiment were identical.

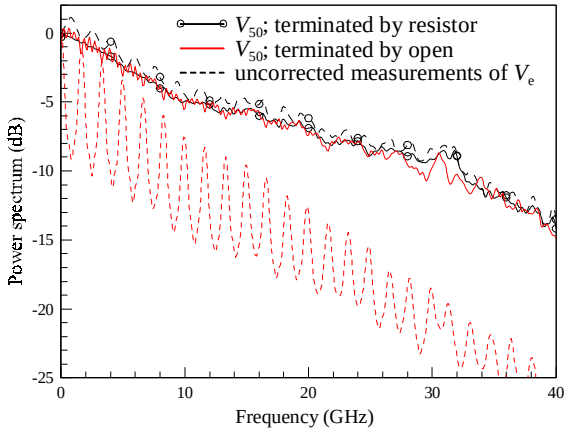

Fig. 3. A comparison of the corrected power spectra of V_{50} for the two waveforms shown in Fig. 2. The uncorrected spectra of V_e are shown in dashed lines. The curves are normalized to 0 dB at DC.

We use the sampling beam to reconstruct the distorted electrical waveform in the CPW. We pass this sampling beam through a variable optical delay, linearly polarize it at an angle of 45° to the x-axis of the $LiTaO_3$, and then focus it through a small gap in our coplanar line, as illustrated in Fig. 1. The electric field between the CPW conductors changes the polarization of the optical beam passing through the wafer. We chop the excitation beam and use a lock-in amplifier to detect this change in optical polarization. By changing the delay of the sampling beam, we incrementally adjust the relative time at which the optical sampling pulse reaches the surface of the wafer: we are thus able to trace out the electrical waveform on the wafer as it evolves with time.

II. Mismatch Corrections

Figure 2 shows two sampled voltage waveforms measured in the substrate between the center conductor and one of the ground planes of the CPW by our electro-optic sampling system. Both waveforms were generated by the same photoreceiver under the same bias and excitation conditions. However, one of the waveforms was measured in a CPW terminated with an open circuit, while the other was measured in a CPW terminated with a planar resistor with a DC resistance of 34.8 Ω. The figure shows that the CPW resistor sharpens the main pulse and quickly, although not entirely, dampens the multiple reflections.

To correct for the frequency response of the probe head, for its connection to the lossy and dispersive CPW, and for the CPW termination, we used the method described in [1]. We first performed a coaxial frequency-domain short-open-load-thru (SOLT) vector-network-analyzer calibration at the coaxial reference plane in the system, and then measured the reflection coefficient $\Gamma_s(f)$ of the photoreceiver over the frequency range 0-40 GHz.

We then performed a second-tier multiline thru-reflect-line (TRL) vector-network-analyzer calibration [3] whose reference plane corresponded to the point at which the electro-optic measurements were made, and set the reference impedance to 50 Ω using the method of [4]. This calibration is based on direct broadband measurements of the traveling waves in the CPW, and avoids systematic errors inherent in on-wafer SOLT calibrations. We measured the reflection coefficient $\Gamma_L(f)$ of the CPW terminations with this calibration and determined the scattering parameters $S_{ij}(f)$ of the probe head from the "error boxes" determined by the second-tier TRL calibration [5].

We used standard transformations [5] to

detremine the admittances Y_s of the photoreceiver and Y_L of the CPW load and the admittance parameters Y_{ij} of the probe head from Γ_s, Γ_L , and S_{ij}. Finally, we constructed the equivalent circuit shown in Fig. 1, which is based on these measured quantities.

To determine the photoreceiver's Norton equivalent current I_N in the frequency domain, we first obtained the Fourier transform $V_e(f)$ of the time-domain waveform $v_e(t)$ measured by the electro-optic sampling system. Then, using Kirchhoff's laws, we calculated the internal current $I_{12}(f)$ from

$$I_{12} = V_e(Y_L + Y_{22} + Y_{12}), \quad \textbf{(1)}$$

the voltage V_s at the coaxial reference plane from

$$V_s = I_{12} Y_2^{-1}, \quad \textbf{(2)}$$

and the photoreceiver's Norton equivalent current I_N from

$$I_N = V_s(Y_s + Y_{11} + Y_{12} + Y_2), \quad \textbf{(3)}$$

where

$$Y_2 \equiv \left[-Y_{12}^{-1} + (Y_{22} + Y_{12} + Y_L)^{-1}\right]^{-1}. \quad \textbf{(4)}$$

From I_N we can obtain the photoreceiver's Thévenin equivalent voltage $V_T(f)$ and the voltage $V_{50}(f)$ that the photoreceiver would generate across a perfect 50 Ω load at the coaxial reference plane from

$$V_T \equiv \frac{I_N}{Y_s} = I_N Z_s \; ; \quad V_{50} = V_T \frac{50}{50 + Z_s}, \quad \textbf{(5)}$$

where $Z_s \equiv Y_s^{-1}$ is the photoreceiver's electrical source impedance.

Figure 3 compares the power spectra V_e of the uncorrected waveform measured by the electro-optic sampling system to that of V_{50}, the voltage the photoreceiver would deliver to a perfect 50 Ω coaxial load. Figure 3 shows two comparisons corresponding to the two time-domain waveforms of Fig. 2. The corrections not only reduce the "ripple" due to the multiple reflections in the measurements, but they also correct rigorously for the attenuation and distortion of the probe head, and for the broadening and narrowing of the main pulse caused by the two different CPW terminations.

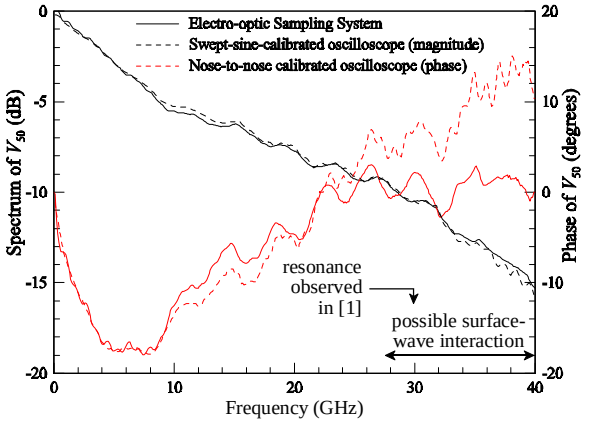

Fig. 4. Comparison of calibrated oscilloscope measurements to an electro-optic-sampling-system measurement.

III. Systematic Errors

Our electro-optic sampling system does not exactly measure the voltage on the wafer, but rather measures a voltage waveform that is slightly broadened by the finite response time of the $LiTaO_3$ substrate, a finite optical pulse width and optical beam waist, penetration of the electric field into the substrate, and multiple optical reflections in the substrate. The errors due to these mechanisms increase roughly quadratically below 40 GHz. Table 1 contains our estimates of coefficients describing these systematic errors and uncertainties.

To derive the coefficients in Table 1, we used an autocorrelator to estimate the width of our optical excitation and sampling pulses, and transmission through small holes to estimate the beam waist of the optical sampling beam. We estimated the effect of multiple optical reflections inside the substrate from the index of refraction of the $LiTaO_3$ substrate. Finally, we performed full-wave electromagnetic calculations using the method of [6] to estimate the time that the optical sampling pulses spend traversing the CPW's decaying electric field, which penetrates approximately 100 µm into the $LiTaO_3$ substrate.

Multiple optical reflections in the substrate can

be eliminated with optical coatings, and it is easy to calculate and correct for the broadening of the measured voltage due to the finite transit time of the optical sampling pulses through the CPW electric field in the substrate. Thus we believe that ultimately we should be able to reduce our systematic measurement uncertainties to about $\pm 7\times10^{-6}$ dB/GHz^2 and $\pm 3\times10^{-6}$ degrees/GHz^2, well below our ability to accurately perform the mismatch corrections.

IV. Preliminary Comparison to Calibrated Oscilloscope Measurements

Figure 4 compares our electro-optic measurement of V_{50} to measurements we performed with a commercial sampling oscilloscope. We corrected the oscilloscope's magnitude response with the "swept-sine" calibration [7] and its phase response with the "nose-to-nose" calibration [8], [9], as implemented in [7]. We normalized the magnitudes to extrapolate to 0 dB at DC and averaged waveforms from the detector while the excitation beam was being chopped, as explained in [1]. We also averaged voltages in the two gaps to suppress the 30 GHz resonance observed in [1], which we believe to be a slot-mode resonance.

The slot-mode resonance and the existence of microstrip-like surface-wave modes supported by the thick $LiTaO_3$ substrate currently limit the bandwidth of our electro-optic measurements to 30 GHz. Nevertheless, despite the imperfect mismatch corrections and a low signal-to-noise ratio, the measurements agree well to 30 GHz.

Table 1: Systematic-Error Estimates

Error mechanism	magnitude dB/GHz^2	phase deg/GHz^2
$LiTaO_3$ response time	$<10^{-7}$	$<10^{-8}$
optical pulse width	-1.2×10^{-6}	0
optical beam waist	-3×10^{-7}	0
multiple reflections	-4×10^{-4}	$\pm10^{-3}$
CPW field penetration	-1.4×10^{-5}	$+5\times10^{-6}$

References

[1] D.F. Williams, P.D. Hale, T.S. Clement, and J.M. Morgan, "Mismatch corrections for electro-optic sampling systems," *56th Automatic RF Techniques Group Conf. Dig.*, Boulder, CO, Nov. 20-Dec. 1, 2000.

[2] B.H. Kolner and D.M. Bloom, "Electrooptic sampling in GaAs integrated circuits," *IEEE Jour. Quantum Electron.*, vol. QE-22, no. 1, pp. 79-93, Jan. 1986.

[3] R.B. Marks, "A Multiline Method of Network Analyzer Calibration," *IEEE Trans. Microwave Theory Tech.*, vol. 39, no. 7, pp. 1205-1215, July 1991.

[4] R.B. Marks and D.F. Williams, "Characteristic Impedance Determination using Propagation Constant Measurement," *IEEE Microwave Guided Wave Lett.*, vol. 1, no. 6, pp. 141-143, June 1991.

[5] R. B. Marks and D. F. Williams, "A general waveguide circuit theory," *J. Res. Natl. Inst. Stand. Technol.*, vol. 97, no. 5, pp. 533-562, Sept.-Oct., 1992.

[6] W. Heinrich, "Full-wave analysis of conductor losses on MMIC transmission lines," *IEEE Trans. Microwave Theory Tech.*, vol. MTT-38, no. 10, pp. 1468-1472, Oct. 1990.

[7] P.D. Hale, T.S. Clement, K.C. Coakley, C.M. Wang, D.C. DeGroot, and A.P. Verdoni, "Estimating the magnitude and phase response of a 50 GHz sampling oscilloscope using the 'nose-to-nose' method," *55th ARFTG Conference Digest*, June 2000.

[8] J. Verspecht and K. Rush, "Individual characterization of broadband sampling oscilloscopes with a nose-to-nose calibration procedure," *IEEE Trans. Instrum. Meas.*, vol. 43, no. 2, pp. 347-354, April 1994.

[9] K. Rush, S. Draving, and J. Kerley, "Characterizing high-speed oscilloscopes," *IEEE Spectrum*, pp. 38-39, September 1990.